Electrodynamics of carbon nanotubes: Dynamic conductivity, impedance boundary conditions, and surface wave propagation

G. Ya. Slepyan and S. A. Maksimenko
Institute of Nuclear Problems, Belarus State University, Bobruiskaya str. 11, Minsk 220050, Belarus

A. Lakhtakia
CATMAS—Computational and Theoretical Materials Sciences Group, Department of Engineering Science and Mechanics, Pennsylvania State University, University Park, Pennsylvania 16802-1401

O. Yevtushenko
Institute of Radiophysics and Electronics, National Academy Sciences of Ukraine, Ak. Proskura str. 12, Kharkov 310085, Ukraine and Max-Planck-Institut für Physik komplexer Systeme, Nöthnitzer Str. 38, 01187 Dresden, Germany

A. V. Gusakov
Institute of Nuclear Problems, Belarus State University, Bobruiskaya str. 11, Minsk 220050, Belarus
(Received 16 March 1999)

Effective boundary conditions, in the form of two-sided impedance boundary conditions, are formulated for the linear electrodynamics of single- and multishell carbon nanotubes (CN's). The impedance is derived using the dynamic conductivity of CN's, which is obtained for different CN's (zigzag, armchair, and chiral) in the frame of the semiclassical as well as quantum-mechanical treatments. Propagation of surface waves in CN's is considered. The phase velocities and the slow-wave coefficients of surface waves are explored for a wide frequency range, from the microwave to the ultraviolet regimes. Relaxation is shown to qualitatively change the dispersion characteristics in the low-frequency limit, thereby rendering the existence of weakly retarded plasmons impossible. A dispersionless propagation regime is shown possible for the surface waves in the infrared regime. Attenuation and retardation in metallic and semiconductor CN's are compared.
[S0163-1829(99)16247-7]

I. INTRODUCTION

Since the discovery by Iijima[1] of quasi-one-dimensional crystalline structures of carbon atoms generally referred to as carbon nanotubes (CN's), several unique physical properties have been predicted theoretically and detected experimentally. Much accumulated information is available in several review papers and monographs.[2–7] CN's are classified by the dual index (m,n). The two integers m and n represent the vector characterizing the way of turning a planar sheet into a nanotube, with $n=0$ for zigzag CN's, $n=m$ for armchair CN's, and $0<n\neq m$ for chiral CN's.

Electronic properties of, and electron transport in, CN's became the focus of numerous studies.[8–14] These properties of CN's are quite different from those of well-known carbonic structures such as a planar monatomic graphite sheet (also called *graphene*). Perhaps the most attractive result was to establish a correlation between a CN's conductivity and its geometrical configuration. A carbon nanotube can manifest either metallic or semiconductor properties, depending on its cross-sectional radius and geometric chiral angle. This correlation arises from the transverse quantization of charge carrier motion and is coupled with the quasi-one-dimensional topology of CN's.

Several researchers have now begun to focus their attentions on electromagnetic processes in CN's,[5,15–22] and two main lines of investigations can be recognized. The first is aimed at wave processes in multi-CN samples incorporating either regular or irregular ensembles of CN's[5,15–18]; the other concerns the electrodynamics of single CN's.[19–22]

(i) Multi-CN samples—i.e., distrbutions of CN inclusions in some host material—furnish typical examples of particulate composite materials. As such, their analysis[5,15–18] involves the following general procedure: The effective constitutive parameters of the homogenized composite material are evaluated using various field-averaging algorithms at frequencies below some upper limit, taking the difference between the local and the homogenized fields into account as exhibited by, e.g., the Mossotti-Clausius formalism.[16] A comprehensive description of the electromagnetic response properties of these composite materials, with the effect of chirality included, was presented recently by Tasaki *et al.*[15]

(ii) Several publications[19–22] can be assigned to the second main line of investigations. The polarizability tensor of a single CN per unit length was determined by Benedict *et al.*[22] Both π and σ plasmons in CN's of different kinds, including multi-shell coaxial CN's, were considered by Jiang[20] and Yannouleas *et al.*[21] The occurrence of surface electromagnetic waves at infrared frequencies in nanotubes was predicted and their dispersion characteristics were described by us elsewhere.[19]

Although both lines of investigation are strongly intertwined, they are not equivalent. On the one hand, the effective constitutive parameters of a particulate composite material are indeed dictated by the properties of single inclusions and the host material. On the other hand, certain properties

of inclusions are not manifested by composite materials because of homogenization, and some other properties of composites appear solely due to interaction between inclusions.[23,24] The electrodynamics of a single nanotube is of special interest not only for homogenization of composite materials, but also because experimental methods are available to separate a single nanotube from others and to measure its individual properties.[25,26]

In this paper, we model the electromagnetic response properties of a single CN through effective boundary conditions. This model is widely applied in microwave electronics and antenna theory, e.g., for the design of semi-transparent screens and helical sheaths in traveling wave tubes.[27,28] In a predecessor paper,[19] we initiated the application of this approach to nanotubes. It entails the replacement of a real nanotube by a continuous, infinitely thin, cylindrical surface on which two-sided impedance boundary conditions for the electromagnetic field are laid down. The surface impedance tensor is expressed in terms of the dynamic conductivity of the nanotube.

Three assumptions in the derivation of the dynamic conductivity put restrictions on the applicability of our earlier results[19] to real CN's as follows:

(i) In the framework of a spiral model, the real honeycomb crystalline structure of graphite was implemented as a tetragonal lattice. While that assumption is adequate for BC_2N nanotubes, its application to CN's is not always satisfactory.

(ii) The effect of the transverse quantization of electron momentum was neglected. Hence, our earlier results are applicable to CN's with large cross-sectional radii (so that the dynamic conductivity is close to that of graphene).

(iii) The semiclassical approximation was used to describe electron motion, which is applicable only in the infrared regime.

Our aim for this paper was to eliminate the three assumptions, so that results of more general applicability would emerge. Therefore, we considered eigenwaves—including surface waves—in CN's and thereby extended the applicability of our model to the optical and the ultraviolet regimes, wherein electromagnetic processes exhibit pronounced peculiarities.

This paper is arranged as follows: In Sec. II, the dynamic conductivities of CN's of different kinds are evaluated, taking into account the actual crystalline structure of CN's, the transverse quantization of electron momentum, and the quantum-mechanical nature of electron motion. Comparison is made with our previous results.[19] The equivalent boundary conditions for a single-shell CN are then formulated in Sec. III. Corrections due to spatial dispersion are estimated. A similar approach is developed in Sec. IV for multishell nanotubes with coaxial geometry. An analysis of eigenwaves in CN's, predicated on the equivalent boundary conditions, is provided in Sec. V. Special attention is paid to their attenuation coefficients over a wide spectral range (covering from the microwave to the ultraviolet regimes). The paper concludes with a discussion in Sec. VI.

Parenthetically, we use a two-dimensional (2D) cartesian coordinate system (x,y) for graphene; and the circular cylindrical coordinate system (ρ,ϕ,z) for any CN, with the CN axis parallel to the z axis. The x axis is oriented along the hexagon side. The transition from graphene to a zigzag CN is established by the substitution $\{x\to z, y\to\phi\}$; while the transition from graphene to an armchair CN requires the substitution $\{y\to z, x\to\phi\}$.

II. AXIAL DYNAMIC CONDUCTIVITY OF A NANOTUBE

A. Preliminaries

To begin with, let us outline our general approach. On applying the semiclassical approximation to describe the motion of π-electrons exposed to the electromagnetic field of a transversely symmetric (i.e., $\partial/\partial\phi\equiv 0$) surface wave in a single-shell CN, a distribution function $f(\mathbf{p},z,t)$ becomes applicable. It satisfies the Boltzmann kinetic equation

$$\frac{\partial f}{\partial t}+eE_z\frac{\partial f}{\partial p_z}+v_z\frac{\partial f}{\partial z}=J[F(\mathbf{p});f(\mathbf{p},z,t)], \tag{1}$$

where $\mathbf{p}$ is the electron's two-dimensional quasimomentum tangential to the CN's surface, p_z is the projection of $\mathbf{p}$ on the axis of the CN, $v_z=\partial\mathcal{E}/\partial p_z$, $\mathcal{E}=\mathcal{E}(\mathbf{p})$ is the electron energy with respect to the Fermi level, and $J(F;f)$ is the collision integral. The chemical potential of graphite being null-valued,[10] the Fermi equilibrium distribution function

$$F(\mathbf{p})=\frac{1}{1+\exp\left\{\dfrac{\mathcal{E}(\mathbf{p})}{k_BT}\right\}} \tag{2}$$

involves only the Boltzmann constant k_B and the temperature T. In the so-called momentum-independent relaxation time approximation,[29] the collision integral is given by

$$J[F(\mathbf{p});f(\mathbf{p},z,t)]=\nu[F(\mathbf{p})-f(\mathbf{p},z,t)], \tag{3}$$

where ν is the relaxation frequency. Conventionally, ν is assumed to be constant and equal to the reciprocal for the time of the electron mean-free path; see Jishi *et al.*[8] for a numerical estimate of $1/\nu$ for armchair CN's from microscopic considerations.

Let us set $E_z=\Re[E_z^0e^{i(hz-\omega t)}]$ in the Boltzmann kinetic equation (1), where h is the axial wavenumber (not to be confused with the Planck constant $\hbar$) and ω is the angular frequency of the exciting electromagnetic field. Setting $f=F+\Re[\delta f e^{i(hz-\omega t)}]$ with δf as a small quantity to be found, and keeping only linear terms in E_z^0, we then obtain

$$\delta f=-i\frac{\partial F}{\partial p_z}\frac{eE_z^0}{\omega-hv_z+i\nu}. \tag{4}$$

The axial surface current density $J_z=\Re[J_z^0e^{i(hz-\omega t)}]$ is to be determined by the relation

$$J_z=\frac{2e}{(2\pi\hbar)^2}\int\int v_z f\,d^2\mathbf{p}, \tag{5}$$

with e as the electron charge. Using both foregoing equations, we get

$$J_z^0=\tilde{\sigma}_{zz}(\omega,h)E_z^0, \tag{6}$$

wherein

$$\tilde{\sigma}_{zz}(\omega,h)=-i\frac{2e^2}{(2\pi\hbar)^2}\int\int\frac{\partial F}{\partial p_z}\frac{v_z d^2\mathbf{p}}{\omega-hv_z+i\nu} \tag{7}$$

is the axial conductivity. As $\tilde{\sigma}_{zz}$ is the axial conductivity *evaluated semiclassically*, it must be distinguished from the total axial conductivity σ_{zz} considered in Sect. II F.

Equation (7) is applied to zigzag and armchair CN's in Secs. II B and II C, wherein the electron dispersion relation $\mathcal{E}(\mathbf{p})$ as well as the range of the $\mathbf{p}$ integration are needed. For the sake of tractability, now we neglect the effect of spatial nonlocality by setting $h=0$ in Eq. (7). Physically, this neglect means that the third term on the left side of Eq. (1) is discarded, just as we did elsewhere.[19] The role of this nonlocality is discussed in Sec. III.

B. Zigzag nanotubes

The electron dispersion relation for CN's can be formulated in the framework of the tight-binding model, in strict analogy with the counterpart relation[10,11,30,31]

$$\mathcal{E}(\mathbf{p})=\pm\gamma_0\sqrt{1+4\cos\left(\frac{3bp_x}{2\hbar}\right)\cos\left(\frac{\sqrt{3}bp_y}{2\hbar}\right)+4\cos^2\left(\frac{\sqrt{3}bp_y}{2\hbar}\right)} \tag{8}$$

for a planar monatomic sheet with hexagonal lattice. Here, the overlap integral $\gamma_0=2.7$ eV for carbon, and $b=1.42$ Å is the interatomic distance in a graphite sheet. The positive and the negative signs in Eq. (8) correspond to the conduction and the valence bands, respectively. The range of the quasimomentum $\mathbf{p}$ (the first Brillouin zone) is confined to the hexagons shown in Figs. 1(a) and 1(b).

A fundamental distinction between CN's and graphene is in the transverse quantization of charge-carrier motion,[10,11] which causes p_x and p_y to exhibit discrete spectra. In order to derive the dispersion relation for zigzag CN's—classified by the dual index $(m,n=0)$[2,3]—from Eq. (8), we observe that the x and y directions in Eq. (8) correspond to the z and ϕ directions. The substitution $\{p_x\rightarrow p_z, p_y\rightarrow p_\phi\}$ is implemented in Eq. (8) therefore. Simultaneously, p_ϕ is quantized as follows:

$$p_\phi=\frac{2\pi\hbar s}{\sqrt{3}mb},\quad s=1,2,\ldots,m. \tag{9}$$

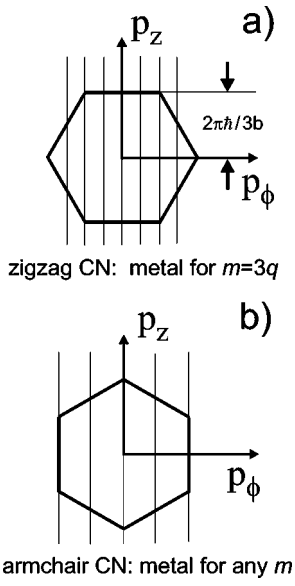

FIG. 1. Configuration of the first Brillouin zone for (a) zigzag and (b) armchair CN's.

The range of $\mathbf{p}$ is transformed thus into the population of straight line segments (9) located inside the hexagons shown in Fig. 1(a).

The electron dispersion relation for zigzag CN's thus takes the following form:

$$\mathcal{E}(p_z,s)=\pm\gamma_0\sqrt{1+4\cos\left(\frac{3bp_z}{2\hbar}\right)\cos\left(\frac{\pi s}{m}\right)+4\cos^2\left(\frac{\pi s}{m}\right)}. \tag{10}$$

On neglecting interband transitions between states with different values of s, Eq. (7) reduces to

$$\tilde{\sigma}_{zz}(\omega,0)=-\frac{4i\pi\hbar e^2 n_0}{\sqrt{3}mb(\omega+i\nu)F_0}\times\sum_{s=1}^{m}\int_{-2\pi\hbar/3b}^{2\pi\hbar/3b}v_z^2(p_z,s)\frac{\partial F}{\partial\mathcal{E}}dp_z, \tag{11}$$

where n_0 is the surface density of conduction-band electrons in graphene, and

$$F_0=\int\int_{1\text{stBZ}}F(\mathbf{p})d^2\mathbf{p}. \tag{12}$$

The range qualifier $_{1\text{stBZ}}$ refers to the first Brillouin zone.

In the limiting case of a CN with infinitely large cross-sectional radius (i.e., as $m\rightarrow\infty$), the spectrum of allowed values of p_ϕ is continuous and the summation over s in Eq. (11) transforms to an integration over the hexagon in Fig. 1(a). Physically, this means that the dynamic axial conductivity of a CN becomes *locally* equivalent to the dynamic conductivity of graphene, as $m\rightarrow\infty$. Consequently, Eq. (11) simplifies to

$$\tilde{\sigma}_{zz}(\omega,0)=-2ie^2n_0\frac{1}{(\omega+i\nu)F_0}\int\int_{1\text{stBZ}}v_z^2(\mathbf{p})\frac{\partial F}{\partial\mathcal{E}}d^2\mathbf{p}. \tag{13}$$

Here and hereafter, we denote $\tilde{\sigma}_{zz}(\omega,0)$ simply as $\tilde{\sigma}_{zz}$ for notational simplicity.

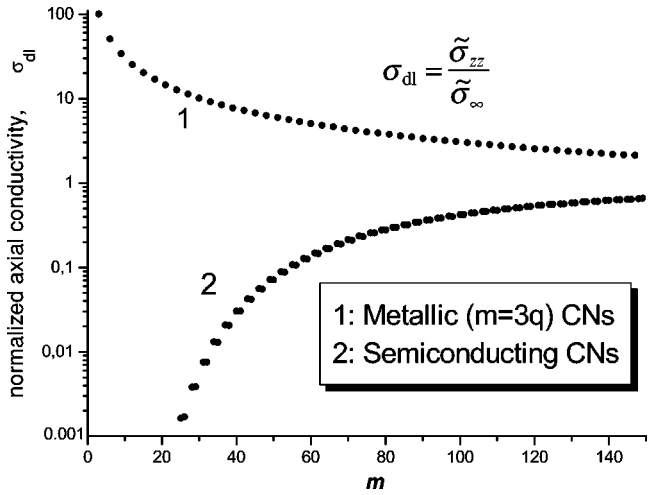

FIG. 2. Normalized semiclassical conductivity $\tilde{\sigma}_{zz}/\tilde{\sigma}_{\infty}$ for zigzag CN's as a function of m (and therefore of the cross-sectional radius R); $\tilde{\sigma}_{\infty}=\lim_{m\to\infty}\tilde{\sigma}_{zz}$, $\gamma_0=2.7$ eV, $\tau=3\times10^{-12}$ s and $T=264$ K.

The integral in Eq. (13) can be analytically estimated asymptotically with respect to the large parameter $\lambda=\gamma_0/k_BT$, taking into the account that the proximal regions of the vertices of the hexagon in Fig. 1(a) provide the main contribution to these integrals. These vertices are the so-called Fermi points (where $\mathcal{E}=0$). By analogy with Wallace,[31] in the vicinity of these points the approximation

$$\mathcal{E}(\mathbf{p})\simeq\pm\frac{3\gamma_0 b}{2\hbar}|\mathbf{p}-\mathbf{p}_F| \tag{14}$$

is applied, with $\mathbf{p}_F$ as the constant quasimomentum corresponding to the particular Fermi point.

The rest of the integration procedure is as follows: The idea is to pass from the integration over $\mathbf{p}$ to the integration over $\mathcal{E}$ and ϕ, extending the integration over $0\leqslant\mathcal{E}<\infty$. Using Eqs. (2) and (14), and taking into account that $d^2\mathbf{p}=(2\hbar/3b\gamma_0)^2\mathcal{E}d\mathcal{E}d\phi$ as per Wallace,[31] we find

$$\int\int_{1\text{stBZ}} v_z^2(\mathbf{p})\frac{\partial F}{\partial\mathcal{E}}d^2\mathbf{p}$$

$$\cong-\frac{1}{2k_BT}\int_0^{\infty}\frac{\mathcal{E}d\mathcal{E}}{\cosh^2\left(\frac{\mathcal{E}}{2k_BT}\right)}\int_0^{2\pi}\sin^2\phi d\phi$$

$$=-2\pi k_BT\ln 2. \tag{15}$$

In the same fashion, from Eq. (12) we get

$$F_0=(2\pi\hbar)^2n_0/2\simeq\frac{4\pi}{27}\left(\frac{\pi\hbar}{\lambda b}\right)^2. \tag{16}$$

In view of the foregoing equations, the estimate

$$\tilde{\sigma}_{zz}\simeq i\frac{27\ln 2}{\pi^2}\left(\frac{eb}{\hbar}\right)^2\frac{\gamma_0\lambda}{\omega+i\nu}n_0=i\frac{2\ln 2}{\pi\hbar^2}\frac{e^2k_BT}{\omega+i\nu} \tag{17}$$

easily emerges in the limit $m\to\infty$.

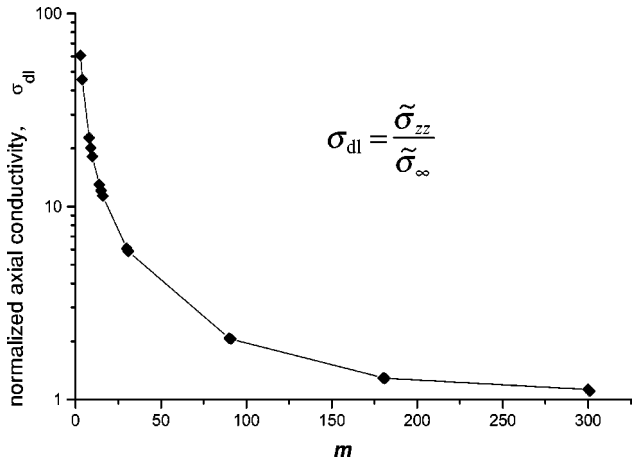

FIG. 3. Same as Fig. 2, but for armchair CN's.

For finite m, the integration on the right side of Eq. (11) was performed numerically. Figure 2 shows the dependence of $\tilde{\sigma}_{zz}$ on m. Because the radius R of a zigzag CN is connected to m by the linear relation $R=\sqrt{3}mb/2\pi^5$, the curves in Fig. 2 really present the dependence of σ_{zz} on the cross-sectional radius. As R increases ($m>300$), $\tilde{\sigma}_{zz}$ approaches an asymptotic value, which agrees well with that given by the asymptotic formula (17), which corresponds to the dynamic conductivity of semimetallic graphene.[31] The fact that CN's are metallic at $m=3q$ (with q as an integer)[32] manifests itself in sharp discontinuities of $\tilde{\sigma}_{zz}$ at those values of m. Let us note that at $m=3q$, two of the integration lines for the right side of Eq. (11) go through the Fermi points, resulting in the drastic growth of the numerical value of the integral. At $m\neq3q$, $\tilde{\sigma}_{zz}$ lies in a range typical of semiconductors.

The dynamic conductivity of metallic CN's is easily estimated analytically for small m. The integration in Eq. (11) is approximately accomplished under assumption that the main contribution is provided by the lines passing through the Fermi points $s=m/3$ and $s=2m/3$. Using the simplest approximation for the dispersion relation in the vicinity of the Fermi points, such as Eq. (14), we transform the integration over p_z to that over $\mathcal{E}$ and carry it out over the range $0\leqslant\mathcal{E}<\infty$; thus,

$$\sum_s\int_{-2\pi\hbar/3b}^{2\pi\hbar/3b}v_z^2(p_z,s)\frac{\partial F(p_z,s)}{\partial\mathcal{E}}dp_z$$

$$\cong4\int_0^{2\pi\hbar}v_z^2(p_z,m/3)\frac{\partial F(p_z,m/3)}{\partial\mathcal{E}}dp_z$$

$$\cong-\frac{3b}{2\hbar}\frac{\gamma_0}{k_BT}\int_0^{\infty}\frac{d\mathcal{E}}{\cosh^2\left(\frac{\mathcal{E}}{2k_BT}\right)}=-\frac{3\gamma_0 b}{\hbar}. \tag{18}$$

After using Eqs. (18) and (16), the result

$$\tilde{\sigma}_{zz}\simeq i\frac{2\sqrt{3}e^2\gamma_0}{m\pi\hbar^2(\omega+i\nu)},\quad m=3q, \tag{19}$$

emerges. The estimates given by Eq. (19) are in reasonable accord with exact values for $m<60$.

Let us compare Eqs. (17) and (19). Both show identical frequency-dependences, but not temperature-dependences. Equation (19) contains only one temperature-dependent quantity (*viz.*, the relaxation frequency ν), whereas Eq. (17) includes an additional linear dependence on T. As per Eq. (19), $\tilde{\sigma}_{zz}$ depends on the radius R (*via* m) for small R; but Eq. (17) clearly shows that $\tilde{\sigma}_{zz}$ is independent of the CN geometry for large-radius CN's.

C. Armchair nanotubes

In order to evaluate the electron dispersion relation for armchair nanotubes—classified by the dual index $(m,n=m)$—from Eq. (11), the substitution $\{p_x\rightarrow p_\phi, p_y\rightarrow p_z\}$ must be carried out with

$$p_\phi=\frac{2\pi\hbar s}{3mb}, \quad s=1,2,\ldots,m; \tag{20}$$

accordingly,

$$\mathcal{E}(p_z,s)=\pm\gamma_0\sqrt{1+4\cos\left(\frac{\pi s}{m}\right)\cos\left(\frac{\sqrt{3}bp_z}{2\hbar}\right)+4\cos^2\left(\frac{\sqrt{3}bp_z}{2\hbar}\right)}. \tag{21}$$

Following the procedure described in Sec. II B, Eq. (7) reduces to

$$\tilde{\sigma}_{zz}=-\frac{4\pi\hbar ie^2n_0}{3mb(\omega+i\nu)F_0}\sum_{s=1}^{m}\int_{-2\pi\hbar/\sqrt{3}b}^{2\pi\hbar/\sqrt{3}b}v_z^2(p_z,s)\frac{\partial F}{\partial\mathcal{E}}dp_z \tag{22}$$

at $h=0$ for armchair CN's.

For $R=3mb/2\pi$ being small, $\tilde{\sigma}_{zz}$ is analytically estimated from Eq. (21) by considering only the contribution of the line passing through the Fermi point $s=m$. Further manipulations, analogous to that for Eq. (18), lead to the estimate

$$\tilde{\sigma}_{zz}\simeq i\frac{2e^2\gamma_0}{m\pi\hbar^2(\omega+i\nu)} \tag{23}$$

for armchair CN's. Let us note that Eq. (23) differs from Eq. (19) only by the factor $\sqrt{3}$. However, unlike Eq. (23), Eq. (19) is applicable at any value of m below a certain limit.

Figure 3 shows the plot of $\tilde{\sigma}_{zz}$ versus m calculated numerically *via* Eqs. (21) and (22). As $m\rightarrow\infty$, the conductivity of armchair CN's approaches the asymptotic value for zigzag CN's. An analytical estimate of the right side of Eq. (22), carried out by the method presented in Sec. II B, substantiates that conclusion. As $m\rightarrow\infty$, Eqs. (21) and (22) reduce to Eqs. (8) and (17), respectively. This is in agreement with the in-plane conductivity of graphene being isotropic.[31]

At finite m, the behavior of $\tilde{\sigma}_{zz}$ as a function of m is drastically different for zigzag and armchair CN's. Indeed, unlike for zigzag CN's, the dependence is monotonic for armchair CN's. Physically, this follows from the fact that armchair CN's are conductors at any m, while zigzag CN's can be either metallic or semiconducting. For $m<50$, the approximate Eq. (23) fits well the results computed from Eq. (21).

D. Chiral nanotubes

A fundamental feature which distinguishes chiral CN's from zigzag and armchair CN's is in the manifestation of the so-called chiral current.[13,14,19] In a chiral CN $(0<n\neq m)$, an applied axial electric field induces the current to flow along a helical line. The axial and azimuthal components of the surface current density are given, respectively, by $J_z^0=\tilde{\sigma}_{zz}E_z^0$ and $J_\phi^0=\tilde{\sigma}_{\phi z}E_z^0$ where $\tilde{\sigma}_{\phi z}$ is the chiral conductivity of the chiral CN evaluated semiclassically. A first-principles numerical simulation of $\tilde{\sigma}_{\phi z}$ was carried out by Miyamoto *et al.*,[13] whereas phenomenological modeling was presented by us elsewhere.[14,19] Both approaches led to the same conclusion that chiral conductivity is rather small when compared to the axial conductivity. As a result, the current chiral angle $\gamma=\tan^{-1}(J_z/J_\phi)$ is close to $\pi/2$, but that conclusion is invalid when nonlinear effects come to play.[14]

The approximate analytical expression

$$\tilde{\sigma}_{zz}\simeq i\frac{2\sqrt{3}e^2\gamma_0}{\pi\hbar^2\sqrt{m^2+mn+n^2}(\omega+i\nu)} \tag{24}$$

is available for metallic chiral CN's $(2m+n=3q)$,[32] using a method similar to that for deriving Eqs. (19) and (23). Equation (24) reduces to Eq. (19) for $n=0$ and to Eq. (23) for $m=n$. Equation (24) and the relation $\tilde{\sigma}_{\phi z}=0$ describe electrodynamic properties of chiral conducting CN's, in the simplest approximation. The evaluation of $\tilde{\sigma}_{zz}$ for chiral CN's wth arbitrary indices m and n has to be carried out numerically from Eq. (7).

E. Comparison with the spiral model

Let us now compare our obtained results with the predictions of the phenomenological spiral (helicoidal) model of Romanov and Kibis[12] we had used earlier.[14,19] In this model, a CN is treated as a periodic chain of carbon atoms strung on a helix with b as the period, and the real honeycomb crystalline structure of graphite is ignored. But, owing to its simplicity, the spiral model is analytically tractable. In particular, this model was applied to analyze electron structure[12] and to describe electron transport[14] in CN's.

The linear dynamic conductivity of a chiral CN was derived using the spiral model by us earlier.[19] Let us now compare that result (in the achiral limit) with Eq. (17). In the achiral limit, the helical atomic chain is transformed to a

periodic system of coaxial atomic rings with the same distance between the atoms in a ring as between two adjacent rings. In the tight-binding approximation, the electron dispersion relation for this structure is given by

$$\mathcal{E}(\mathbf{p})=\Delta\left[2-\cos\left(\frac{p_z b}{\hbar}\right)-\cos\left(\frac{p_\phi b}{\hbar}\right)\right], \tag{25}$$

where Δ is the overlap integral (~ 2 eV for carbon). Both p_z and p_ϕ vary arbitrarily within the first Brillouin zone,[33] as the transverse quantization of electron motion was not considered earlier[19]). Equation (25) allows exact evaluation of the integrals in Eq. (7), after setting $F=\exp[-\mathcal{E}(\mathbf{p})/k_BT]$, $\nu=\text{const}$, and $h=0$. This results in[19]

$$\tilde{\sigma}_{zz}=i\left(\frac{eb}{\hbar}\right)^2\frac{\hat{n}_0\Delta}{\omega+i\nu}\frac{I_1(\Delta/k_BT)}{I_0(\Delta/k_BT)}, \tag{26}$$

where $I_0(\cdot)$ and $I_1(\cdot)$ are modified Bessel functions, and $\hat{n}_0$ is the surface density of free electrons in the conduction band.

When $\Delta \gg k_BT$ the main contribution to integral in Eq. (7) comes from the neighborhood of the point $\mathbf{p}=\mathbf{0}$ where $\mathcal{E}(\mathbf{p})=0$. In this region, the approximation

$$\mathcal{E}(\mathbf{p})\simeq\frac{\Delta b^2}{2\hbar^2}|\mathbf{p}|^2, \tag{27}$$

similar to Eq. (14), turns out to be valid. Then, applying the method used for the derivation of Eq. (17), we obtain the expression

$$\tilde{\sigma}_{zz}=i\left(\frac{eb}{\hbar}\right)^2\frac{\hat{n}_0\Delta}{\omega+i\nu}. \tag{28}$$

As the condition $\Delta \gg k_BT$ holds true at room temperature, $I_1(\Delta/k_BT)\simeq I_0(\Delta/k_BT)$ and Eq. (26) reduces to Eq. (28).

Now we can compare Eqs. (17) and (28), taking into account that $n_0\neq\hat{n}_0$. The reason for this inequality is that, by using the approximate dispersion relation (25) for the spiral model, we effectively substitute a square lattice for the actual hexagonal lattice.

The ratio $\hat{n}_0/n_0$ may be evaluated using a method due to Wallace[31] as follows: By definition,

$$n_0\simeq\int_0^\infty N(\mathcal{E})F(\mathcal{E})d\mathcal{E}, \tag{29}$$

where

$$N(\mathcal{E})=2\int\frac{d\Sigma}{|\text{grad}_{\mathbf{p}}\,\mathcal{E}|}, \tag{30}$$

is the density of states, $d\Sigma$ is an infinitely small element of an isoenergetic surface, and the Fermi function defined jointly by Eqs. (2) and (14) is used. The integration in Eq. (30) is carried out over an isoenergetic surface to yield

$$n_0=2\pi/27b^2\lambda^2. \tag{31}$$

Analogous expressions may be written for $\tilde{n}_0$ with the Boltzmann distribution as $F(\mathcal{E})$ and Eq. (27) as the electron dispersion relation. The multiplier 2 is omitted from the analog of Eq. (30), because $\tilde{n}_0$ in the spiral model[19] is the density of conduction electrons, whereas n_0 accounts for charge-carriers of both signs (i.e., holes and electrons). Simple manipulations then yield

$$\hat{n}_0=k_BT/\pi b^2\Delta. \tag{32}$$

Therefore, we derive the ratio

$$\frac{\hat{n}_0}{n_0}=\frac{27\gamma_0\lambda}{2\pi^2\Delta}, \tag{33}$$

so that Eq. (28) is rewritten as follows:

$$\tilde{\sigma}_{zz}\simeq i\frac{27}{2\pi^2}\left(\frac{eb}{\hbar}\right)^2\frac{\gamma_0\lambda}{\omega+i\nu}n_0. \tag{34}$$

The right sides of Eqs. (34) and (17) differ only by the constant factor $2\ln 2$. This remarkable coincidence strongly suggests that the spiral model adequately describes the conductivity of large-radius CN's, and can be useful for qualitative estimates of $\tilde{\sigma}_{zz}$.

At this stage, let us emphasize an important fact: for the most part, the spiral model adequately reflects the properties of doped nanotubes such as BC_2N; while the foregoing hexagonal dispersion relations hold for pure carbon nanotubes. Therefore, this section provides a comparison of the conductivity of doped and carbon nanotubes with different structure.

F. The role of interband transitions

Consideration of interband transitions entails the abandonment of the semiclassical approximation, and the Liouville equation[34,35] for the density matrix must replace the classical Boltzmann equation. Alternatively, in order to find the conductivity of a single CN, we use the rigorous quantum-mechanical treatment of effective permittivity of a CN-based composite material, as reported by Tasaki *et al.*[15] and Lin and Shung.[18] An expression for the axial conductivity of a single CN then emerges easily. Following Tasaki *et al.*[15] and a previous paper of ours,[16] we get

$$\sigma_{zz}=\omega\alpha_{zz}/2i\pi R=-i\omega[\epsilon_{zz}(\omega)-1]/4\pi S\rho_T, \tag{35}$$

where α_{zz} is the axial polarizability of a single CN; $\epsilon_{zz}(\omega)$ is the axial component of the permittivity tensor of the CN-based composite material; while S is the surface area of a CN and ρ_T is the volumetric density of CN's.

On using the known expression of $\epsilon_{zz}(\omega)$,[18,15] the relation

$$\sigma_{zz}=\tilde{\sigma}_{zz}+\Delta\sigma \tag{36}$$

is obtained for the *total* axial conductivity. Here, $\tilde{\sigma}_{zz}$ is the semiclassical version evaluated in previous subsections, while

$$\Delta\sigma=\frac{ie^2(\omega+i\nu)}{2\pi^2\hbar R}\sum_s\int_{1stBZ}\frac{1}{\mathcal{E}(p_z,s)}|\theta_{cv}(p_z,s)|^2 \times\frac{F[-\mathcal{E}(p_z,s)]-F[\mathcal{E}(p_z,s)]}{\hbar^2(\omega+i\nu)^2-4\mathcal{E}^2(p_z,s)}dp_z \tag{37}$$

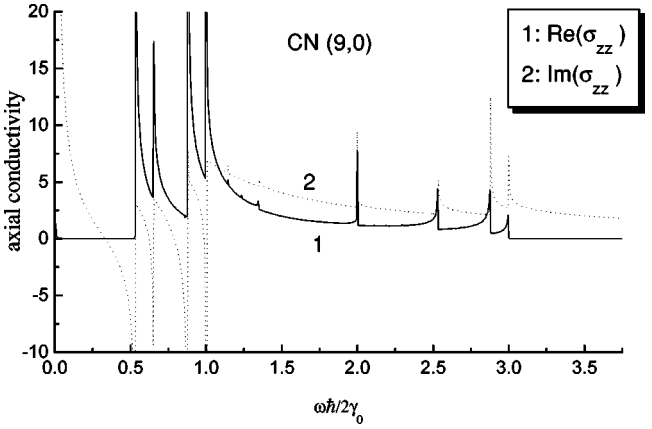

FIG. 4. Frequency-dependence of the total axial conductivity of the (9,0) metallic zigzag CN; $\gamma_0=2.7$ eV, $\tau=3\times10^{-12}$ s, and $T=295$ K. Axial conductivity is normalized by $e^2/2\pi\hbar$.

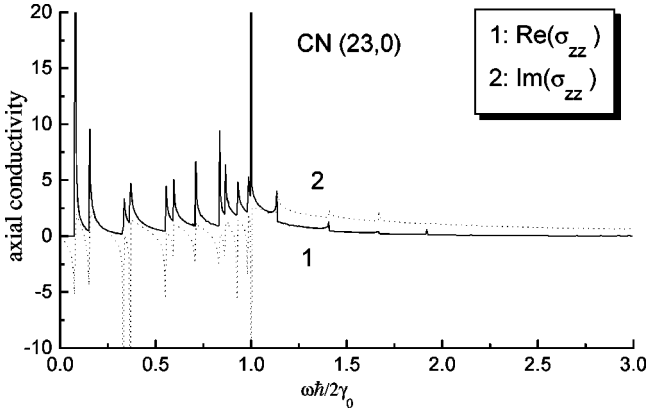

FIG. 5. Same as Fig. 4, but for the (23,0) semiconducting zigzag CN.

describes the contribution of transitions between the conduction and valence bands. In the last expression, θ_{cv} is the matrix element of the longitudinal velocity, which can be approximately evaluated by the formula[18,37]

$$|\theta_{cv}|=\hbar^{-1}|\Im[\sqrt{H_{12}^{*}/H_{12}}\partial H_{12}/\partial p_z]| \tag{38}$$

with $H_{12}(p_z,s)$ as the matrix element of the Hamiltonian of electrons in a hexagonal lattice given by Lin and Shung.[18]

In the microwave and the infrared frequency regimes, where $\hbar\omega\ll\gamma_0$, the first term on the right side of Eq. (36) is dominant—which justifies the use of the semiclassical approach in those regimes. As the frequency increases, the second term catches up with the first one in magnitude and then becomes greater. Neglecting the contribution of free charge-carriers[36] and assuming $T\to0$, we then recover the results of Lin and Shung;[18] in that case, the first term on the right side of Eq. (36) is rejected, while $F(-\mathcal{E})=1$ and $F(\mathcal{E})=0$ are set in Eq. (37).

In the high-frequency regime, where $(\hbar\omega)^2\gg4\gamma_0^2$, Eq. (37) yields

$$\Delta\sigma\simeq\frac{ie^2G}{\hbar^2(\omega+i\nu)}, \tag{39}$$

where

$$G=\frac{1}{2\pi^2\hbar R}\sum_{s=1}^{m}\int_{1\text{st BZ}}\frac{|\theta_{cv}(p_z,s)|^2}{\mathcal{E}(p_z,s)}\{F[-\mathcal{E}(p_z,s)] -F[\mathcal{E}(p_z,s)]\}dp_z. \tag{40}$$

Thus, on comparing Eqs. (39) and (13), we see that the frequency-dependence on the right side of Eq. (39) turns out to be similar to that the semiclassical term. This implies that the electron energy in the high-frequency field exceeds significantly the interband transition energies so that the motion of charge-carriers becomes quasi-free.

The plots in Figs. 4 and 5 represent the characteristic frequency-dependences of $\sigma_{zz}(\omega)$ for two zigzag CN's, one of which is metallic while the other is semiconducting. The contribution of free charge-carriers to $\Re[\sigma_{zz}]$ is dominant at low frequencies, but is too small to be evident in both figures. The initial decline of $\Im[\sigma_{zz}]>0$ with increasing frequency in Fig. 4 is certainly due to free charge-carriers, but the same feature is absent from Fig. 5 because of the low density of free charge-carriers in semiconductors. As the frequency increases, $\Im[\sigma_{zz}]$ intersects the zero line and becomes negative. This change in sign is due to interband electronic transitions. Optical resonances appear with further increase in frequency, the frequency of the lowest resonance decreasing as the CN radius R grows. For the same R, a semiconducting CN resonates at a lower frequency than a metallic CN.

Let us end this section by analytical estimate for the low-frequency edge of the optical transition band. Such an estimate can be obtained from the general approximate relation for the density of electron states derived by Mintmire and White:[38] The ocation of the first singularity on the density of state curve calculated by them[38] allows one to conclude that

$$\hbar\omega<\begin{cases}3\gamma_0 b/2R, & \text{metallic CN's;}\\ \gamma_0 b/2R, & \text{semiconducting CN's.}\end{cases} \tag{41}$$

This finding correlates well with the results presented in Figs. 4 and 5 for nanotubes of different radius and different type of conductivity. The fact that the estimate (41) gives the correct values at the low-frequency edge of the optical transition band shows its usefulness and justifies its applicability to nanotubes of different types.

III. EFFECTIVE BOUNDARY CONDITIONS FOR CARBON NANOTUBES EXPOSED TO SPATIALLY NONHOMOGENEOUS FIELDS

The spatial nonhomogeneity of electromagnetic field leads to the dependence of f on z that is reflected by the third term on the left side of Eq. (1) as well as by the dependence of σ_{zz} on h in Eq. (7). Let us now derive the boundary conditions for electromagnetic field on a CN's surface, assuming the spatial nonhomogeneity to be small. This assumption allows us to expand the denominator of the integrand in Eq. (7) into a power series with respect to h. Only terms of even powers contribute to the integration over $\mathbf{p}$. Restricting further to the quadratic term with respect to h, we obtain

TABLE I. Magnitude of the spatial dispersion parameter $\tilde{l}_0$ for different zigzag CN's.

CN index	(17,0)	(25,0)	(31,0)	(43,0)	(100,0)	(250,0)	$(3q,0)$	$(\infty,0)$
$\tilde{l}_0(c/v_F)^2$	0.15	0.25	0.31	0.35	0.51	0.67	1.0	0.75

$$\tilde{\sigma}_{zz}(\omega,h)=\tilde{\sigma}_{zz}(\omega,0)-i\frac{2e^2}{(2\pi\hbar)^2}\frac{h^2}{(\omega+i\nu)^3}\int\int v_z^3\frac{\partial F}{\partial p_z}d^2\mathbf{p}, \tag{42}$$

where $\tilde{\sigma}_{zz}(\omega,0)$ was derived in Sec. II; equivalently,

$$J_z^0=\tilde{\sigma}_{zz}(\omega,0)E_z^0-i\frac{2e^2}{(2\pi\hbar)^2}\frac{h^2E_z^0}{(\omega+i\nu)^3}\int\int v_z^3\frac{\partial F}{\partial p_z}d^2\mathbf{p}. \tag{43}$$

The second term on the right side of Eq. (42) is small. Therefore, we substitute $E_z^0\simeq J_z^0/\sigma_{zz}(\omega,0)$ in the second term on the right side of Eq. (43) to get

$$J_z^0=\tilde{\sigma}_{zz}(\omega,0)E_z^0+\frac{h^2}{k^2(1+i\nu/\omega)^2}\tilde{l}_0J_z^0, \tag{44}$$

where $k=\omega/c$ is the wave number in free space, and

$$\tilde{l}_0=\frac{1}{c^2}\int\int v_z^4\frac{\partial F}{\partial\mathcal{E}}d^2\mathbf{p}\left[\int\int v_z^2\frac{\partial F}{\partial\mathcal{E}}d^2\mathbf{p}\right]^{-1}. \tag{45}$$

Applying for zigzag and armchair CN's—with the respective electron dispersion relations (10) and (21)—we transform Eq. (45) to

$$\tilde{l}_0=\frac{1}{c^2}\sum_s\int v_z^4(p_z,s)\frac{\partial F(p_z,s)}{\partial\mathcal{E}}dp_z \times\left[\sum_s\int v_z^2(p_z,s)\frac{\partial F(p_z,s)}{\partial\mathcal{E}}dp_z\right]^{-1}. \tag{46}$$

The integrals in Eq. (45) may be estimated using the method applied in Sec. II to determine $\sigma_{zz}(\omega,0)$. Then, as $m\to\infty$, the right side of Eq. (46) reduces to a constant; i.e.,

$$\tilde{l}_0\simeq\frac{3}{4}\left(\frac{v_F}{c}\right)^2, \tag{47}$$

where $v_F=3\gamma_0 b/2\hbar$. For metallic CN's with not too large m, the estimate $\tilde{l}_0\sim10^{-5}$ is given by Eq. (46), after using Eq. (14) and summing over only the lines intersecting the Fermi points. In other cases, numerical evaluation of the integrals must be carried out. Some computational results are presented for zigzag CN's in Table I.

Recalling the connection between E_z and E_z^0, etc., we formulate the dynamic conductivity equation

$$J_z+\frac{\tilde{l}_0}{k^2(1+i\nu/\omega)^2}\frac{\partial^2J_z}{\partial z^2}=\tilde{\sigma}_{zz}E_z \tag{48}$$

from Eq. (44). But the surface current density

$$J_z=\lim_{\delta\to0}\frac{c}{4\pi}(H_\phi|_{\rho=R+\delta}-H_\phi|_{\rho=R-\delta}) \tag{49}$$

(in Gaussian units), so that the boundary condition

$$\lim_{\delta\to0}\left[1+\frac{\tilde{l}_0}{k^2(1+i\nu/\omega)^2}\frac{\partial^2}{\partial z^2}\right](H_\phi|_{\rho=R+\delta}-H_\phi|_{\rho=R-\delta}) =\frac{4\pi}{c}\tilde{\sigma}_{zz}E_z|_{\rho=R} \tag{50}$$

emerges from Eq. (48). In addition to Eq. (50), E_z must be continuous across the CN surface,[19] i.e.,

$$\lim_{\delta\to0}(E_z|_{\rho=R+\delta}-E_z|_{\rho=R-\delta})=0. \tag{51}$$

Equations (50) and (51) constitute the complete system of boundary conditions for CN's exposed to an axially polarized electric field.

When the electric field is transversely polarized, the boundary conditions

$$\lim_{\delta\to0}(E_\phi|_{\rho=R+\delta}-E_\phi|_{\rho=R-\delta})=0,$$

$$\lim_{\delta\to0}(H_z|_{\rho=R+\delta}-H_z|_{\rho=R-\delta})=0 \tag{52}$$

must be valid at the CN surface in the simplest approximation. The second of Eqs. (52) reflects the neglect of the transverse current. Indeed, Benedict *et al.*[22] showed that the transverse polarizability of any CN is much less than its axial polarizability, thereby allowing us to neglect the transverse surface current density. Parenthetically, Eqs. (50) and (52) are similar to the two-sided impedance boundary conditions for semitransparent screens in the microwave regime.[28]

Analysis of the physical meaning of Eqs. (50)–(52) is in order. Though the CN surface possesses a periodic crystalline structure, Eqs. (50)–(52) incorporate only constant coefficients (i.e., $\tilde{\sigma}_{zz}$ and $\tilde{l}_0$), and are devoid of any periodic functions. This is because the technique of deriving the three equations is equivalent to the averaging of microscopic fields over an infinitesimally small volume. In accordance with Eq. (49), the Maxwell equations with boundary conditions (50)–(52) define spatially averaged currents and electromagnetic fields induced by the currents. These fields are identical to the actual ones at a certain (of the order of b) distance from the CN surface. For that reason, the averaged currents and the actual currents may be treated as equivalent. The technique of macroscopic averaging is similar to one of introducing constitutive parameters for bulk media, but differing in that the averaging occurs in boundary conditions, but not in field equations. Correspondingly, the averaging is carried out over the 2D cylindrical element of CN surface, but not over a 3D element.

The change-over from the semiclassical model to the quantum-mechanical model does not affect the boundary conditions. The only changes necessary are the substitutions $\tilde{\sigma}_{zz} \to \sigma_{zz}$ and $\tilde{l}_0 \to l_0$. Here, σ_{zz} is given by Eq. (36), the coefficient

$$l_0 \simeq \frac{k^2}{2[\epsilon_{||}(\omega,0)-1]} \left. \frac{\partial^2 \epsilon_{||}(\omega,h)}{\partial h^2} \right|_{h=0} (1+i\nu/\omega)^2 \quad (53)$$

appears from the quantum-mechanical treatment, and $\epsilon_{||}(\omega,h)$ is the axial component of the Ehrenreich-Cohen tensor.[39]

IV. EFFECTIVE BOUNDARY CONDITIONS FOR MULTISHELL CARBON NANOTUBES

Present-day technology allows fabrication of multishell CN's of many different kinds.[7] We restrict the analysis to one of the many possible models, which was proposed by Lin and Shung.[5] In this model, a multishell CN is thought of as a set of N coaxial cylindrical single-shell CN's with intershell distance between 3.35 and 3.40 Å.[40] Each shell is characterized by its own dual index (m,n) which is determined by the shell radius. Thus, the geometrical chiral angle changes from one shell to another. Most multishell CN's exhibit metallic properties because they contain single shells of the armchair type.[5]

The basic assumption of the Lin-Shung model is the neglect of intershell interactions. This implies that shell-to-shell jumps of electrons are forbidden, and an electron moves over a particular shell as if all other shells are absent. Assuming these conditions to be valid, we can impose the boundary condition (50) on each shell, while ensuring that σ_{zz} and l_0 change from shell to shell. Thus, in order to investigate the electromagnetic response of a N-shell CN, we will have to separate $N+1$ partial regions and impose Eqs. (50) and (51) at N cylindrical boundaries. This will lead to $2N$ simultaneous algebraic equations, which can be quite cumbersome to handle.

However, a simplified approach is described in Appendix A. This approach is applicable for sufficiently thin CN's of large radius, i.e., when the CN thickness $d=R_{ext}-R_{int}$ is much smaller than the internal and the external radius of the chosen CN. Suppose $N=2$ and the parameters $l_0^{(q)}$ and $\sigma_{zz}^{(q)}, (q=1,2)$ are known. If the illuminating field depends as $\exp(ihz)$ on z, Eq. (50) across each interface reduces to the second relations in Eqs. (A1) and (A2) with

$$\xi_q = \left(1 + \frac{h^2}{k^2(1+i\nu/\omega)^2} l_0^{(i)} \right) \frac{c}{4\pi\sigma_{zz}^{(q)}}, \quad q=1,2. \quad (54)$$

We then consider an *equivalent* single-shell CN of cross-sectional radius $R^{eff}=(R_1+R_2)/2$, and apply the boundary conditions (A1) with ξ_1 replaced by ξ_{eff} defined in Eq. (A8).

The same approach may be adopted when $N>2$; then,

$$\sigma_{zz}^{eff} = \sum_{q=1}^{N} \sigma_{zz}^{(q)}, \quad l_0^{eff} = \sum_{q=1}^{N} l_0^{(q)} \sigma_{zz}^{(q)} \Big/ \sum_{q=1}^{N} \sigma_{zz}^{(q)}. \quad (55)$$

Thus, a multishell CN can be treated as a single shell CN with an *effective radius* and *effective parameters* given by Eq. (55). The distinctions in the electromagnetic response properties of different shells become inconsequential for $m \gg 1$, providing $\sigma_{zz}^{eff} \simeq N\sigma_{zz}^{(1)}$ and $l_0^{eff} \simeq l_0^{(1)}$.

V. SURFACE ELECTROMAGNETIC WAVES IN CARBON NANOTUBES

A. Dispersion equation

As an example of the application of the effective boundary conditions derived in Sec. III, let us emulate the predecessor paper[19] to examine the propagation of surface waves along an isolated, infinitely long CN, the surrounding medium being free space (i.e., vacuum). After neglecting the chiral current, the electromagnetic field of such a wave is expressed in terms of the electric Hertz vector $\mathbf{\Pi}_\epsilon$ as follows:

$$\mathbf{E} = \nabla(\nabla \cdot \mathbf{\Pi}_\epsilon) + k^2 \mathbf{\Pi}_\epsilon, \quad (56)$$

$$\mathbf{H} = -ik\nabla \times \mathbf{\Pi}_\epsilon.$$

The electric Hertz vector has only the axial component and its z dependence is in the form of a traveling wave. Hence, it is represented by

$$\mathbf{\Pi}_\epsilon = A\mathbf{u}_z \begin{Bmatrix} I_l(\kappa\rho)K_l(\kappa R) \\ I_l(\kappa R)K_l(\kappa\rho) \end{Bmatrix} e^{ihz} e^{il\phi}, \quad (57)$$

where A is an amplitude, $\mathbf{u}_z$ is the unit vector in the axial direction, h is the guide wave number to be determined, l is an integer, $\kappa = \sqrt{h^2-k^2}$, while $I_l(\cdot)$ and $K_l(\cdot)$ are the modified Bessel functions.[41] The upper and the lower lines in Eq. (57) correspond to the regions $\rho<R$ and $\rho>R$, respectively.

Equations (56) and (57) automatically satisfy the continuity condition for E_z at $\rho=R$; hence, all we have to do is to fulfill Eq. (50). Substitution of Eqs. (56) and (57) into Eq. (50), followed by the use of the Wronskian of modified Bessel functions,[41] leads to the following dispersion equation with respect to κ:

$$\left(\frac{\kappa}{k}\right)^2 I_l(\kappa R)K_l(\kappa R) = \frac{ic}{4\pi kR\sigma_{zz}} \left[1 - \frac{1+(\kappa/k)^2}{(1+i\nu/\omega)^2} l_0 \right]. \quad (58)$$

Equation (58) is general in its applicability: It is applicable to single shell as well as multishell CN's, whether the surface conductivity model is semiclassical or quantum-mechanical. For a multi-shell CN, R^{eff}, σ_{zz}^{eff}, and l_0^{eff} must be used in lieu of R, σ_{zz}, and l_0, respectively, in Eq. (58).

B. Attenuation

Let us consider surface waves in the infrared regime where the frequency of the illuminating electromagnetic wave significantly exceeds the relaxation frequency (i.e., $\omega \gg \nu$), and the contribution of free electrons to the conductivity is dominant. The attenuation coefficient is small in this regime ($10^{-5} < kb < 10^{-3}$) and can be easily estimated.

Towards that end, let us utilize the fact that the slow-wave coefficient in the infrared regime is small; i.e., $|h|^2 \gg k^2$ and $|\kappa|^2 \gg k^2$. Then, with

$$\check{R}=\kappa R, \quad \alpha(\check{R})=\frac{(kR)^2+l_0\check{R}^2}{(kR)^2-l_0\check{R}^2}, \quad \check{\xi}=\frac{ic}{4\pi\sigma_{zz}(1+i\nu/\omega)}, \tag{59}$$

Eq. (58) is rewritten as follows:

$$\mathcal{Q}(\check{R})=\frac{\check{R}^2 I_l(\check{R})K_l(\check{R})}{1-l_0\check{R}^2/(kR)^2}=kR\check{\xi}\left[1+i\frac{\nu}{\omega}\alpha(\check{R})\right]. \tag{60}$$

In the free-electron approximation, the parameter $\check{\xi}$ is real and positive valued, while the contribution of resonant transitions makes $\check{\xi}$ complex valued.

Since we assumed that $\omega \gg \nu$, the contribution from electron collisions can be treated perturbatively.[42] Let $\check{R}=\check{R}^{(0)}+\delta\check{R}$, where $\check{R}^{(0)}$ is the solution of Eq. (60) for $\nu=0$, and $\delta\check{R}$ is a small correction. Expanding $\mathcal{Q}(\check{R})$ into a Taylor series and taking into account that $\mathcal{Q}(\check{R}^{(0)})=kR\check{\xi}$, we obtain

$$\delta\check{R}\simeq ikR\check{\xi}\nu\left[\omega\left.\frac{d\mathcal{Q}}{d\check{R}}\right|_{\check{R}=\check{R}^{(0)}}\right]^{-1}\alpha(\check{R}^{(0)}). \tag{61}$$

Writing the guide wavenumber as $h=\Re[h]+i\Im[h]$, we then get the attenuation coefficient

$$\Im[h]\simeq\frac{\check{R}^{(0)}}{\Re[h]R^2}\frac{\nu}{\omega}\mathcal{Q}(\check{R}^{(0)})\left[\left.\frac{d\mathcal{Q}}{d\check{R}}\right|_{\check{R}=\check{R}^{(0)}}\right]^{-1}\alpha(\check{R}^{(0)}) \tag{62}$$

from Eq. (61).

When $l_0\simeq 1.07\times10^{-5}$, for instance, $\mathcal{Q}(\check{R})\simeq\check{R}/2$ and $d\mathcal{Q}/d\check{R}\simeq 1/2$ for $\check{R}<0.1$. In this case, the simple ratio

$$\frac{\Im[h]}{\Re[h]}\simeq\frac{\nu}{\omega} \tag{63}$$

results from Eq. (62).

Analytical estimate of the attenuation coefficient appears to be impossible in the low-frequency regime ($\omega\leqslant\nu$). The same situation also holds for the optical resonance regime, whose lower edges is determined from Eq. (8) and whose bandwidth $\hbar\omega\approx 6\gamma_0$. In these regimes, the transcendental Eq. (60) has to be numerically handled in the complex κ plane, as we now discuss.

C. Modes with polar symmetry

As the complex-valued slow-wave coefficient $\beta=k/h$ is conventionally used for surface waves in the literature on microwaves, we change our emphasis now from h to β.

Let us begin by inferring the general characteristics of surface wave propagation from Eq. (60) in the collisionless limit $\nu=0$. Equation (60) has only one real root for a given l, i.e., there is only one surface wave possible with a particular polar symmetry. Since $\check{\xi}>0$ in the free-electron approximation, the condition $\nu=0$ requires the denominator in Eq. (60) to be positive. That condition holds true when $\check{R}<kR/\sqrt{l_0}$, thereby yielding $\beta>\sqrt{l_0}$. The condition $\beta=\sqrt{l_0}$ therefore defines the cut-off frequency for the surface wave. This cut-off respects to the excitation of a one-dimensional acoustic plasmon in Fermi liquid.[43]

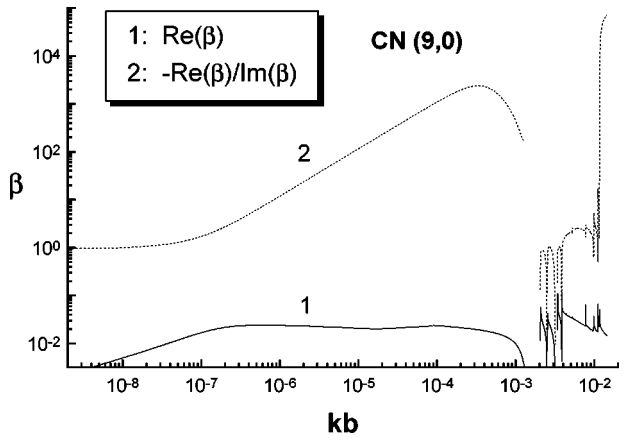

FIG. 6. Frequency-dependence of the complex-valued slow-wave coefficient β for an azimuthally symmetric surface wave in a (9,0) metallic zigzag CN. Input parameter are the same as in Fig. 4.

We turn now to the discussion of numerical results obtained for finite ν. The influence of interband transitions makes $\check{\xi}$ both frequency-dependent and complex-valued. Although knowledge of the relaxation frequency ν is now necessary, the available values of the relaxation time $\tau=1/\nu$ vary significantly from one another.[8,15,43–47] A theoretical estimate for armchair CN's is $\tau\sim 1.4\times10^{-12}$ s at room temperature,[8,45] which is in good agreement with the results of dc measurements[43] ($\tau\simeq 3\times10^{-12}$ s) and microwave measurements[44] ($\tau=10^{-13}$ s). Chauvet *et al.*[46] reported the value $\tau=10^{-13}$ s from electron spin resonance experiments, whereas the estimate $\tau\simeq 4\times10^{-14}$ s was used by Ma and Yuan[47] for zigzag CN's. Finally, the value $\tau\simeq 2\times10^{-14}$ s—which is the relaxation time in ordinary graphite—was used by Tasaki *et al.*[15] for chiral CN's. In the present work, we set $\tau\simeq 3\times10^{-12}$ s.

The frequency-dependences of the slow-wave coefficients of a ϕ-independent wave ($l=0$) are depicted in Figs. 6 and 7 for a metallic CN and a semiconducting CN, respectively. In the low-frequency regime ($\omega\leqslant\nu$) we have $kb<10^{-7}$, so that $\Re[\beta]$ and $\Im[\beta]$ are comparable in value. This indicates that guided surface wave propagation is totally impractical in the low-frequency regime; but that does not mean that CN's are weak conductors of low-frequency electric signals. How-

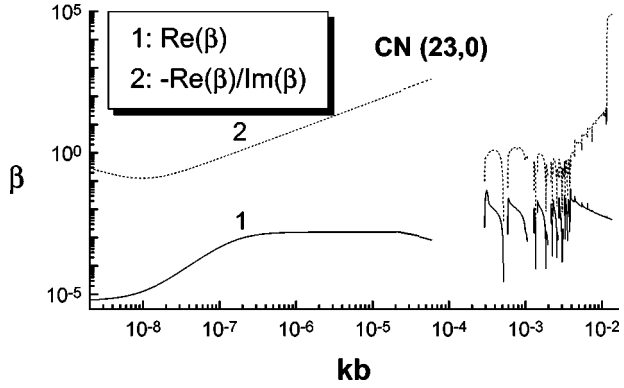

FIG. 7. Same as Fig. 6, but for the (23,0) semiconducting zigzag CN.

ever, it is essential that the condition $h' l_{CN} \ll 1$ holds true at $\omega \leqslant \nu$ for typical CN length $l_{CN} \sim 1$ μm. We conclude that CN's conduct (low-frequency) electrical signals like electric circuits (i.e., unaccompanied by wave processes), which is in accord with general electromagnetic theory.[48]

Weakly attenuated surface waves appear in the infrared regime ($10^{-5} < kb < 10^{-3}$), so that metallic CN's appear very promising for experimental research on surface wave propagation. Figures 6 and 7 show that the retardation $\Re[\beta]$ in a semiconducting CN is smaller than in a metallic CN by an order of magnitude in the chosen spectral regime, but the respective values of $\Im[\beta]$ are comparable. This allows us to conclude that the effect of attenuation in semiconducting CN's far exceeds that in metallic ones. Furthermore, since semiconducting CN's are characterized by large retardation ($2 \times 10^{-3} < \Re[\beta] < 2 \times 10^{-2}$), the electromagnetic field is strongly localized in the vicinity of the CN surface. This means that surface wave propagation in a semiconducting CN is very sensitive to shape deformation. Finally, the phase velocity and the slow-wave coefficient are independent of frequency in the infrared regime. Hence, a infrared wave packet will propagate in a semiconducting CN without distortion, a property of importance for potential applications of CN's in infrared devices.

The situation changes dramatically in the spectral regime of optical resonances. Attenuation substantially increases; and both attenuation and retardation manifest sharp oscillations at resonant frequencies.

In the ultraviolet and the soft x-ray regimes ($kb > 0.01$), conditions for surface wave propagation again becomes appropriate: attenuation significantly decreases and frequency-dependence of β becomes muted. Clearly, that is so, because mainly free electrons are responsible for the conductivity in the ultraviolet/soft x-ray and the infrared regimes.

However, as distinct from the infrared regime, surface wave propagation in the ultraviolet and the soft x-ray regimes is characterized by essential qualitative peculiarities that do not follow from the presented model. First, resonant transitions corresponding to σ electrons appear in the spectrum.[20,21] Second, diffraction by crystalline lattice of CN's comes into play because, owing to strong retardation, the surface wavelength is significantly less than that in free space. For that reason, narrow forbidden gaps arise in the soft x-ray region. These gaps are centered at frequencies determined by the Bragg condition $h(\mathbf{u}_z \cdot \mathbf{e}_d) = N\pi$, where $\mathbf{e}_d$ is an arbitrary lattice vector and N is an integer. For instance, the Bragg condition readily shows that the center frequencies of the first gap for armchair and zigzag CN's are given by the relations $kb = \pi\beta/\sqrt{3}$ and $kb = 2\pi\beta/3$, respectively. Let us also note that, as a CN is electrically large in the ultraviolet and the soft x-ray regimes, macroscopic averaging of the electromagnetic field must be abandoned as also the effective boundary conditions (56). Boundary conditions for unaveraged fields will be analogous to (56), with the axial conductivity σ_{zz} a periodic function of space.[49] Detailed investigation of the contribution of σ-electrons and diffraction by the crystalline lattices of CN's are beyond the scope of the present work.

D. Other modes

Axially nonsymmetric (i.e., $l \neq 0$) surface waves can also propagate in CN's. Qualitatively, their dispersion characteristics are similar to those for axially symmetric surface waves; and, in particular, strong retardation must be mentioned.

The waveguiding properties of CN's should be compared to those of structures—such as metal spirals, dielectric rods and two-wire transmission lines[50]—that are commonplace in the area of microwaves. For instance, in a dielectric rod, a weakly retarded surface wave exists with $l = 1$ at low frequencies, with the field structure resembling a slightly distorted plane wave.[51] In contrast, that surface wave cannot be found in a CN.

In order to elicit the difference between two these structures, let us turn to dispersion equation (60) at $l > 1$, assuming $\breve{R} \ll 1$. As the approximation $I_l(\breve{R}) K_l(\breve{R}) \sim (2l)^{-1}$ then holds true, the solution of Eq. (60) takes the form

$$\breve{R}^2 \simeq 2lkR\breve{\xi}(1 + 2l\breve{\xi} l_0/kR), \tag{64}$$

which yields

$$\beta^2 \simeq \left\{ 1 + \frac{2l\breve{\xi}/kR}{1 + 2l\breve{\xi} l_0/kR} \right\}^{-1}. \tag{65}$$

For a metal spiral and a dielectric rod, the same expression holds, but with the second term in the denominator on the right side of Eq. (65) being negligible compared to unity. Hence, retardation in a metal spiral or a dielectric rod is very small. But the second term is very strong (i.e., $\gg 1$) for a CN, and retardation is therefore high.

Let us now move on to a system of two parallel CN's separated by the distance b_2, which is the nanoscale analog of the well-known two-wire transmission lines.[50] Guided propagation of transverse electromagnetic (TEM) waves is a characteristic of such lines. However, as different from conventional two-wire transmission lines, a TEM wave cannot be guided by the two parallel CN's because of strong retardation. This may be proven by examining the simplest antisymmetric guided wave in the two-CN line, assuming $b_2 \gg R$. The dispersion relation for this wave is obtained by the method of images,[51] which leads to Eq. (60) with

$$\mathcal{Q}(\breve{R}) = \frac{\breve{R}^2 I_0(\breve{R})}{1 - \breve{R}^2 l_0/(kR)^2} [K_0(\breve{R}) - K_0(b_2\breve{R}/R)]. \tag{66}$$

Assuming the condition $\breve{R} \ll 1$ to be satisfied at low frequencies, we come to Eq. (65) where the substitution $1/2l \rightarrow \ln(b_2/R)$ must be performed. The retardation then is quite large, although it is much smaller than the retardation of a surface wave with $l = 1$ in a single CN.

Finally, let us consider the propagation of fast guided waves in hollow metallic waveguides. Such waves also do not exist in single nanotubes even at high frequences ($kR \sim 1$), due to the high transparency of CN's. The parameter ξ_1 involved in boundary condition (A1) ranges in value from 10^3 to 10^5 for realistic CN's, and corresponds to the transmission coefficient $|\breve{t}| \sim 1$ in Eq. (A7). Consequently, a CN can then function only as a highly leaky waveguide.

VI. CONCLUDING REMARKS

In this paper, we presented analytical expressions for the axial dynamic conductivity of CN's, with

(i) the actual hexagonal crystalline structure of carbon accounted for, and

(ii) both semiclassical as well as quantum-mechanical analyses employed.

The derived expressions were correlated with computational results for different types of CN's (zigzag, armchair, chiral), both metallic and semiconducting. Using the developed theory of linear conductivity, we set up effective boundary conditions for the electromagnetic field across a CN surface. We applied these conditions to enlarge our understanding of the electrodynamics of single CN.

Our formalism can be utilized for consideration of diffraction problems in different types of nanotubes, viz., CN's of finite length, bent and corrugated CN's, CN's with junctions, multi-shell CN's with hexagonal cross section,[40] etc. The derived effective boundary conditions can also serve as the basis for description of interaction of CN's with beams of electrons and other charged particles.

The investigation of guided surface wave propagation exemplifies the application of the formalism developed, and it is of significance in its own right too. Such waves can be excited by directing laser or electron beams along a CN axis. These surface waves are characterized by strong retardation and, consequently, have large field gradients in the transverse (i.e., xy) plane. As the result, such surface waves must manifest a strong pondermotive effect and may be of interest, therefore, for laser-control movement of small particles.[52,53]

A comparison of the properties of the guided surface waves considered with those of π plasmons[20,21] yields results of some interest. In the strong retardation regime, $\nabla(\nabla\cdot\vec{\Pi}_\epsilon)$ dominates over $k^2\vec{\Pi}_\epsilon$ in Eq. (56) for the electric field. Neglecting the weaker term and making the substitution $k\approx h$ in Eq. (50), we see that the electric field is described by a quasistatic potential, which is the same as for π plasmons. Thus, the guided surface waves investigated in the present paper and the π plasmons model the same type of electronic excitation in CN's.

However, the results of the two models are not completely equivalent. Jiang[20] and Yannouleas[21] used a hydrodynamic description of the motion of charge carriers, thereby disallowing relaxation processes. As a consequence, wavenumbers h of π plasmons can vary in a wide range, and, in particular, can be small. Our model incorporates a more adequate kinematic theory that involves attenuation too. It follows from our theory that relaxation processes make the small-h regime (weak retardation) totally impractical for guided wave phenomena. Moreover, relaxation processes are essential in the optical regime, wherein resonant transitions come to play.

Our formalism allows us to compare carbon nanowaveguides with electronic waveguides,[54] which are quantum wires placed over metallic planes—e.g., $In_{0.53}Ga_{0.47}As$ wires of rectangular cross-section buried in InP. As per Wesström,[54] plasma waves propagate in such electronic waveguides in the millimeter-wave and the infrared regimes. These plasma waves exhibit some properties analogous to those of guided surface waves in CN's, and we conclude that a CN is an electronic waveguide in the infrared regime. CN's as quantum wires of a special type have been treated by Tans *et al.*;[43] and our comparison substantiates the validity of their approach.

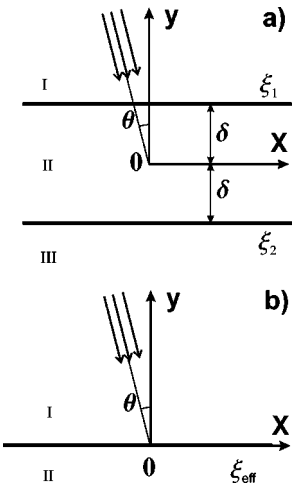

FIG. 8. Schematics of the boundary value problems involving the transmission of a perpendicularly polarized plane-wave incident on (a) two parallel impedance planes, and (b) an equivalent impedance plane.

The interior of a CN can be filled[7] by a medium with a permittivity different from that of free space. This can impart new properties to guided surface wave propagation in CN's. Finally, surface wave propagation can be controlled by external quasielectrostatic and quasimagnetostatic fields, which would alter the surface impedance and, therefore, the waveguiding characteristics of CN's. That exciting prospect will be reported in detail separately.

ACKNOWLEDGMENTS

The research was partially supported through INTAS under Project No. 96-0467 and BMBF under Project No. WEI-001-98.

APPENDIX A

We consider two different boundary values problems and establish their conditional equivalence as follows:

1st boundary value problem

Let a perpendicularly polarized plane wave $\{E_x=E_y=0, H_z=0\}$ be incident at angle θ with respect to the y axis on the system of two infinitesimally thin planes $y=\pm\delta$, as shown in Fig. 8(a). The fields in the three regions—Region I ($y>\delta$), II ($\delta>y>-\delta$) and III ($y<-\delta$)—must satisfy the following boundary conditions:

$$\left.\begin{aligned} E_z^I &= E_z^{II} \\ E_z^I &= i\xi_1(H_x^I - H_x^{II}) \end{aligned}\right\}, \quad y=\delta, \tag{A1}$$

and

$$\left.\begin{aligned} E_z^{II} &= E_z^{III} \\ E_z^{II} &= i\xi_2(H_x^{II} - H_x^{III}) \end{aligned}\right\}, \quad y = -\delta. \tag{A2}$$

Here, the impedances ξ_1 and ξ_2 depend on the angle of incidence θ. The sole cartesian component of the electric field may be represented in the three regions as

$$E_z^I = e^{ikx\sin\theta}(e^{-iky\cos\theta} + \breve{r}e^{iky\cos\theta}), \quad y > \delta,$$

$$E_z^{II} = e^{ikx\sin\theta}(\breve{a}e^{-iky\cos\theta} + \breve{b}e^{iky\cos\theta}), \quad \delta > y > -\delta, \tag{A3}$$

$$E_z^{III} = \breve{t}e^{ik(x\sin\theta - y\cos\theta)}, \quad y < -\delta,$$

where $\breve{r}$, $\breve{t}$, $\breve{a}$, and $\breve{b}$ are unknown amplitudes. Using additionally the magnetic field component $H_x = (ik)^{-1}\partial E_z/\partial y$, in the boundary conditions (A1) and (A2), one can determine all the unknown amplitudes. Most importantly, provided $|k\delta\cos\theta| \ll 1$, we obtain the transmission amplitude

$$\breve{t} \simeq -\frac{2i\cos\theta\dfrac{\xi_1\xi_2}{\xi_1+\xi_2}}{1-2i\cos\theta\dfrac{\xi_1\xi_2}{\xi_1+\xi_2}}. \tag{A4}$$

2nd boundary value problem

Let us now repeat the 1st problem, but for only two regions. Regions I ($y>0$) and II ($y<0$) are separated by the plane $y=0$ on which the following boundary conditions prevail:

$$\left.\begin{aligned} E_z^I &= E_z^{II} \\ E_z^I &= i\xi_{eff}(H_x^I - H_x^{II}) \end{aligned}\right\}, \quad y = 0. \tag{A5}$$

The geometry of the situation is shown in Fig. 8(b). With

$$E_z^I = e^{ikx\sin\theta}(e^{-iky\cos\theta} + \breve{r}e^{iky\cos\theta}), \quad y > 0,$$

$$E_z^{II} = \breve{t}e^{ik(x\sin\theta - y\cos\theta)}, \quad y < 0, \tag{A6}$$

we get

$$\breve{t} = -\frac{2i\xi_{eff}\cos\theta}{1-2i\xi_{eff}\cos\theta}. \tag{A7}$$

Equivalence of the two problems

Clearly, the right sides of Eqs. (A4) and (A7) coincide if we let

$$\xi_{eff} = \frac{\xi_1\xi_2}{\xi_1+\xi_2}. \tag{A8}$$

This shows that a system of two very closely spaced (i.e., $|k\delta\cos\theta| \ll 1$) impedance planes is equivalent (for incident planewaves) to a single impedance plane, with the impedance of the equivalent plane related to the impedances of both actual planes by Eq. (A8). This equivalence leads to the boundary condition transfer technique, which is extremely effective for many multilayered problems.

[1] S. Iijima, Nature (London) **354**, 56 (1991).
[2] M. S. Dresselhaus, G. Dresselhaus, and P. C. Eklund, *Science of Fullerenes and Carbon Nanotubes* (Academic Press, New York, 1996).
[3] *Carbon Nanotubes: Preparation and Properties*, edited by T. W. Ebbesen (CRC Press, Boca Raton, FL, 1997).
[4] M. S. Dresselhaus, G. Dresselhaus, P. Eklund, and R. Saito, Phys. World **11**(1), 33 (1998).
[5] M. F. Lin and K. W.-K. Shung, Phys. Rev. B **51**, 7592 (1995).
[6] S. S. Savinskii and N. V. Khokhryakov, J. Exp. Theor. Phys. **84**, 1047 (1997).
[7] A. V. Eletskii, Phys. Usp. **40**, 899 (1997).
[8] R. A. Jishi, M. S. Dresselhaus, and G. Dresselhaus, Phys. Rev. B **48**, 11 385 (1993).
[9] E. N. Bogachek, M. Jonson, R. I. Shekhter, and T. Swahn, Phys. Rev. B **47**, 16 635 (1993).
[10] M. F. Lin and K. W.-K. Shung, Phys. Rev. B **52**, 8423 (1995).
[11] R. Saito, M. Fujita, G. Dresselhaus, and M. S. Dresselhaus, Phys. Rev. B **46**, 1804 (1992).
[12] D. A. Romanov and O. V. Kibis, Phys. Lett. A **178**, 335 (1993).
[13] Y. Miyamoto, S. G. Louie, and M. L. Cohen, Phys. Rev. Lett. **76**, 2121 (1996).
[14] O. M. Yevtushenko, G. Ya. Slepyan, S. A. Maksimenko, A. Lakhtakia, and D. A. Romanov, Phys. Rev. Lett. **79**, 1102 (1997).
[15] S. Tasaki, K. Maekawa, and T. Yamabe, Phys. Rev. B **57**, 9301 (1998).
[16] A. Lakhtakia, G. Ya. Slepyan, S. A. Maksimenko, O. M. Yevtushenko, and A. V. Gusakov, Carbon **36**, 1833 (1998).
[17] F. J. García-Vidal, J. M. Pitarke, and J. B. Pendry, Phys. Rev. Lett. **78**, 4289 (1997).
[18] M. F. Lin and K. W.-K. Shung, Phys. Rev. B **50**, 17 744 (1994).
[19] G. Ya. Slepyan, S. A. Maksimenko, A. Lakhtakia, O. M. Yevtushenko, and A. V. Gusakov, Phys. Rev. B **57**, 9485 (1998).
[20] X. Jiang, Phys. Rev. B **54**, 13 487 (1996).
[21] C. Yannouleas, E. N. Bogachek, and U. Landman, Phys. Rev. B **53**, 10 225 (1996).
[22] L. X. Benedict, S. G. Louie, and M. L. Cohen, Phys. Rev. B **52**, 8541 (1995).
[23] C. F. Bohren and D. R. Huffman, *Absorption and Scattering of Light by Small Particles* (Wiley, New York, 1983).
[24] *Selected Papers on Linear Optical Composite Materials*, edited by A. Lakhtakia (SPIE Optical Engg. press, Bellingham, WA, 1996).
[25] A. Yu. Kasumov, I. I. Khodos, P. M. Ajayan, and C. Colliex, Europhys. Lett. **34**, 429 (1996).
[26] A. Bezryadin, A. R. M. Verschueren, S. J. Tans, and C. Dekker, Phys. Rev. Lett. **80**, 4036 (1998).
[27] L. A. Weinstein, *The Theory of Diffraction and the Factorization Method* (Golem, New York, 1969).
[28] D. J. Hoppe and Y. Rahmat-Samii, *Impedance Boundary Conditions in Electromagnetics* (Taylor & Francis, Washington, DC, 1995).

[29] F. G. Bass and A. A. Bulgakov, *Kinetic and Electrodynamic Phenomena in Classical and Quantum Semiconductor Superlattices* (Nova, New York, 1997).

[30] L. D. Landau and E. M. Lifshitz, *Electrodynamics of Continuous Media* (Pergamon, Oxford, 1960).

[31] P. R. Wallace, Phys. Rev. **71**, 622 (1947).

[32] The general condition for a CN to be metallic is $|n-m|=3q$, $(q=0,1,2,\ldots)$ (Refs. 10 and 11). Armchair CN's are therefore metallic for any *m*. However, whether a CN is metallic or semiconducting essentially depends on the approximation used to model its electronic properties. B. I. Yakobson and R. E. Smalley [Am. Sci. **85**, 324 (1997)] point out that only armchair CN's are true metals. For zigzag and chiral CN's at $|n-m|=3q$, the gap between the conduction and the valence bands vanishes only in the tight-binding approximation. More adequate modeling shows the existence of a narrow interband gap for any CN with $n\neq m$, but this gap is so narrow that the model of metallic conductivity for such CN's appears justified.

[33] In the model being considered, the first Brillouin zone is determined by the inequality $|p_{z,\phi}|<\hbar\pi/b$.

[34] W. A. Harrison, *Solid State Theory* (McGraw-Hill, New York, 1970).

[35] H. Hang and S. W. Koch, *Theory of the Optical and Electronical Properties of Semiconductors* (World Scientific, Singapore, 1994).

[36] L. G. Johnson and G. Dresselhaus, Phys. Rev. B **7**, 2275 (1973).

[37] The term *free charge-carriers* refers to charge-carriers with energies less than the energies typical of resonant transitions.

[38] J. W. Mintmire and C. T. White, Phys. Rev. Lett. **81**, 2506 (1998).

[39] H. Ehrenreich and M. H. Cohen, Phys. Rev. **115**, 786 (1959).

[40] C.-H. Kiang, M. Endo, P. M. Ajayan, G. Dresselhaus, and M. S. Dresselhaus, Phys. Rev. Lett. **81**, 1869 (1998).

[41] M. A. Abramowitz and I. A. Stegun, *Handbook of Mathematical Functions* (Dover Press, New York, 1972).

[42] A. S. Ilyinsky, G. Ya. Slepyan and A. Ya. Slepyan, *Propagation, Scattering, and Dissipation of Electromagnetic Waves* (Peter Peregrinus, London, 1993).

[43] S. J. Tans, M. H. Devoret, H. Dai, A. Thess, R. E. Smalley, L. J. Geerligs, and C. Dekker, Nature (London) **386**, 474 (1997).

[44] P. Petit, E. Jouguelet, J. E. Fischer, A. Thess, and R. E. Smalley, Phys. Rev. B **56**, 9275 (1997).

[45] C. L. Kane, E. J. Mele, R. S. Lee, J. E. Fischer, P. Petit, H. Dai, A. Thess, and R. E. Smalley, A. R. M. Verschueren, S. J. Tans, and C. Dekker, Europhys. Lett. **41**, 683 (1998).

[46] O. Chauvet, L. Forro, W. Bacsa, D. Ugarte, B. Doudin, and W. A. de Heer, Phys. Rev. B **52**, R6963 (1995).

[47] J. Ma and R.-k. Yuan, Phys. Rev. B **57**, 9343 (1998).

[48] C. H. Durney and C. C. Johnson, *Introduction to Modern Electromagnetics* (McGraw-Hill, New York, 1969).

[49] The situation here is analogous to that in the diffraction theory of x-rays; see: Z. G. Pinsker, *Dynamical Scattering of X-rays in Crystals* (Springer, Berlin, 1978). All notions developed in this theory regarding the permittivity, are applicable to the surface conductivity of CN's.

[50] D. S. Jones, *Acoustic and Electromagnetic Waves* (Clarendon, Oxford, 1986).

[51] L. A. Weinstein, *Electromagnetic Waves* (Sov. Radio, Moscow, 1988)

[52] V. G. Minogin and V. S. Letokhov, *Laser Light Pressure on Atoms* (Gordon & Breach, New York, 1987).

[53] Y. R. Shen, *The Principles of Nonlinear Optics* (Wiley, New York, 1984).

[54] J.-O. J. Wesström, Phys. Rev. B **54**, 11 484 (1996); *ibid.* **58**, 10 351 (1998).